SPACE-DEPENDENT CALCULATIONS OF THE BÖHNEL MULTIPLICITY MOMENTS FOR CYLINDERS

Imre Pázsit and Victor Dykin
Division of Subatomic, High Energy and Plasma Physics
Chalmers University of Technology,
SE-412 96 Göteborg, Sweden

Abstract

At the last two INMM conferences, the theory of and results from a general transport theory calculation of the factorial moments of the number of neutrons emitted spontaneously from a sample were presented. In contrast to the original derivations, made in the so-called point model, in the transport model the spatial and angular dependence of the internal fission chain is taken into account with a one-speed transport theory treatment. Quantitative results were given for a spherical item, and the bias of the point model what regards the estimation of the fission rate, as compared to the more exact space-dependent model, was estimated as a function of the size of the sphere and the alpha factor. In the present work the formalism, as well as the quantitative work, is extended to the treatment of items with cylindrical shapes, which are more relevant in many practical applications. Results are presented for both "square" ($H = D$), as well as for flat and tall cylinders. This way the differences between the cylinder and the sphere on one hand, and that between the various cylinder shapes can be estimated. The results show that the bias depends on the geometry of the item, and similarly to the case of the sphere, the bias of the point model is quite significant for larger item sizes and alpha values, as well as it is non-conservative (underestimates the fissile mass).

1 INTRODUCTION

In a couple of recent publications [1, 2, 3], we have introduced a theoretical framework for the calculation of the multiplicity moments (often referred to as the Böhnel moments), in which, unlike the usual point model derivations [4, 5], the spatial transport was taken into account in a one-speed transport theory model. A one-speed master transport equation was set up for the probability distribution of the number of neutrons leaving the sample, from which the factorial moments can be calculated. Concrete forms of the moment equations were given for a spherical item, and these were solved numerically by a collision number (Neumann-series) type iterative scheme.

The purpose of the present paper is to extend the quantitative work to the calculation of the moments for an item with cylindrical shape. This is motivated by the fact that the cylindrical shape is more realistic in practical cases. On the computational side, the cylindrical geometry obeys fewer symmetry properties, hence the formalism includes more variables an requires more computational effort. In addition, cylinders can have a different H/D ratio (aspect ratio), hence, the difference between the different cylindrical geometries can also be investigated.

2 GENERAL PRINCIPLES

In our previous work [1, 2, 3] a backward-type transport master equation was derived for the scalar generating function

$$g(z|\,\boldsymbol{r}) = \sum_{n=0}^{\infty} z^n\, p(n|\,\boldsymbol{r}) \tag{1}$$

of the number distribution $p(n|\,\boldsymbol{r})$ of neutrons emitted from the sample after a chain initiated by one single starting neutron in position $\boldsymbol{r}$ with an isotropic angular distribution. The equation reads as

$$g(z|\,\boldsymbol{r}) = z\,g_0(z|\,\boldsymbol{r}) + \frac{1}{4\pi}\int_{4\pi} \mathrm{d}\boldsymbol{\Omega} \int_0^{\ell(\boldsymbol{r},\boldsymbol{\Omega})} \mathrm{d}s\, e^{-s}\, q_r\,[g(z|\,\boldsymbol{r'})] \tag{2}$$

where

$$g_0(z|\,\boldsymbol{r}) = \frac{1}{4\pi}\int_{4\pi} \mathrm{d}\boldsymbol{\Omega}\, e^{-\ell(\boldsymbol{r},\boldsymbol{\Omega})}, \tag{3}$$

$\boldsymbol{r'}(s) \equiv \boldsymbol{r} + s\boldsymbol{\Omega}$, $\ell(\boldsymbol{r},\boldsymbol{\Omega})$ is the distance to the boundary of the item from point $\boldsymbol{r}$ along the direction $\boldsymbol{\Omega}$ in units of the mean free path, and $q_r(z)$ is the generating function of the number distribution of neutrons in induced fission in the sample, the quantity in the square brackets being its argument. It is assumed that the only reaction the neutrons undergo is fission.

In a similar way, the expression for the generating function $G(z)$ of the source event induced distribution reads as

$$G(z) = \frac{1}{V}\int_V \mathrm{d}\boldsymbol{r}\, q_s\,[\,g(z|\,\boldsymbol{r})]\,. \tag{4}$$

where $q_s(z)$ is the generating function $p_s(n)$ of the number distribution of the neutrons born in spontaneous fission or in an (α, n) reaction. Hence $p_s(n)$ is a weighted average of the distribution $p_{sf}(n)$ of the neutrons emitted in spontaneous fission and the $p_\alpha = \delta_{1,n}$ of the (α, n) neutrons, the weighting factor being expressed in terms of the so-called α ratio $\alpha = Q_\alpha/F\,\nu_{sf,1}$, where Q_α is the intensity of (α, n) reactions, F is the intensity of the spontaneous fission events, and $\nu_{sf,1}$ is the expectation of the number of neutrons from spontaneous fission.

In an application, the detection rates of the singles, doubles and triples are used, which are simply and directly related to the first three factorial moments of the source event induced emissions. Equations for these factorial moments can be obtained by differentiating (2) and (4) with respect to z, solving the arising integral equations for the moments of the single neutron induced distributions from (2), and integrating them in the expressions obtained from (4).

The equations above are quite general and applicable to any geometry. The choice of the geometry of the item will affect the functional form of $\ell(\boldsymbol{r},\boldsymbol{\Omega})$ as a function of its arguments, as well as the symmetry properties, as well as (through the possible symmetries of the arrangement) the number of spatial and angular co-ordinates for which the integrations need to be performed. For the case of the sphere, the spatial coordinates only included the radial position, and the angular dependence was described by the cosine of the polar angle of the neutron direction vector enclosed with the position vector. For the case of the cylinder, the situation is more involved, as will be described below.

3 EQUATIONS FOR CYLINDRICAL GEOMETRY

Let the radius of the cylinder be R and its height H, measured in units of the mean free path. In cylindrical coordinates, the position of the neutron is defined by $\boldsymbol{r} = \{r, h\}$, and its velocity direction by $\boldsymbol{\Omega} = \{\mu, \varphi\}$, where $\mu = \cos\vartheta$, ϑ being the polar angle. Due to the azimuthal symmetry, all quantities, such as the generating functions $g(z|\,\boldsymbol{r},\boldsymbol{\Omega})$ and $g(z|\,\boldsymbol{r})$ as well as its factorial moments, will not depend on the azimuthal coordinate of the position vector. Hence, all quantities will only depend on the four variables $\{r, h, \mu, \varphi\}$.

Without going into details of the derivation (for the details we refer to Ref. [6]), the distance $\ell(r, h, \mu, \varphi)$ from a point to the boundary of the cylinder in a given direction is found as the

maximum value of s with which both conditions

$$r'(s) = \sqrt{r^2 + s^2\,(1-\mu^2) + 2\,r\,s\sqrt{1-\mu^2}\cos\varphi} \le R \tag{5}$$

and

$$0 \le h'(s) = h + s\,\mu \le H \tag{6}$$

are fulfilled. As soon as any of the above two inequalities is violated, it means that the path crossed either the side, or the top/bottom of the cylinder.

The equation for the scalar generating function $g(z\,|\,r,h)$ of the single neutron induced distribution reads as

$$g(z\,|\,r,h) = z\,g_0(z\,|\,r,h) \,+ \frac{1}{4\pi}\int_{-1}^{1}\mathrm{d}\mu\int_{0}^{2\pi}\mathrm{d}\varphi\int_{0}^{\ell(r,h,\mu,\varphi)}\mathrm{d}s\,e^{-s}\,q_r[g(z\,|\,r'(s),h'(s)] \tag{7}$$

with

$$g_0(z\,|\,r,h) = \frac{1}{4\pi}\int_{-1}^{1}\mathrm{d}\mu\int_{0}^{2\pi}\mathrm{d}\varphi\,e^{-\ell(r,h,\mu,\varphi)}. \tag{8}$$

The equation for the generating function of the source event induced distribution is given as

$$G(z) = \frac{2}{R^2\,H}\int_0^R r\,\mathrm{d}r\int_0^H \mathrm{d}h\,q_s[g(z\,|\,r,h)]. \tag{9}$$

The equations for the moments can be derived by taking the derivatives of the generating functions $g_0(z\,|\,r,h)$ and $G(z)$ of Eqs (7) and (9) at $z=1$, respectively. For consistency, the same notational conventions will be used for the various moments as in our previous work, that is the first, second and third factorial moments of the single neutron induced distribution will be denoted as $n(r,h)$, $m(r,h)$ and $w(r,h)$, respectively. Likewise, the first three factorial moments of the source event induced distribution will be denoted as N, M and W. With these notations, the following equations are obtained for the moments.

First moments

Single neutron induced expectation:

$$n(r,h) = n_0(r,h) \,+ \frac{\nu_{r,1}}{4\pi}\int_{-1}^{1}\mathrm{d}\mu\int_{0}^{2\pi}\mathrm{d}\varphi\int_{0}^{\ell(r,h,\mu,\varphi)}\mathrm{d}s\,e^{-s}\,n(r'(s),h'(s)); \tag{10}$$

with

$$n_0(r,h) = \frac{1}{4\pi}\int_{-1}^{1}\mathrm{d}\mu\int_{0}^{2\pi}\mathrm{d}\varphi\,e^{-\ell(r,h,\mu,\varphi)}; \tag{11}$$

Source event induced expectation:

$$N = \frac{2\,\nu_{s,1}}{R^2\,H}\int_0^R r\,\mathrm{d}r\int_0^H \mathrm{d}h\,n(r,h) \tag{12}$$

Second moments

$$m(r,h) = A(r,h) + \frac{\nu_{r,1}}{4\pi}\int_{-1}^{1}\mathrm{d}\mu\int_{0}^{2\pi}\mathrm{d}\varphi\int_{0}^{\ell(r,h,\mu,\varphi)}\mathrm{d}s\,e^{-s}\,m(r'(s),h'(s)) \tag{13}$$

with

$$A(r,h) = \frac{\nu_{r,2}}{4\pi} \int_{-1}^{1} \mathrm{d}\mu \int_{0}^{2\pi} \mathrm{d}\varphi \int_{0}^{\ell(r,h,\mu,\varphi)} \mathrm{d}s\, e^{-s}\, n^2(r'(s), h'(s)) \tag{14}$$

and

$$M = \frac{2}{R^2 H} \int_{0}^{R} r\,\mathrm{d}r \int_{0}^{H} \mathrm{d}h \left\{ \nu_{s,2}\, n^2(r,h) + \nu_{s,1}\, m(r,h) \right\} \tag{15}$$

Third moments

$$w(r,h) = B(r,h) + \frac{\nu_{r,1}}{4\pi} \int_{-1}^{1} \mathrm{d}\mu \int_{0}^{2\pi} \mathrm{d}\varphi \int_{0}^{\ell(r,h,\mu,\varphi)} \mathrm{d}s\, e^{-s}\, w(r'(s), h'(s)) \tag{16}$$

with

$$B(r,h) = \frac{1}{4\pi} \int_{-1}^{1} \mathrm{d}\mu \int_{0}^{2\pi} \mathrm{d}\varphi \int_{0}^{\ell(r,h,\mu,\varphi)} \mathrm{d}s\, e^{-s} \left\{ \nu_{r,3}\, n^3(r'(s), h's)) + 3\,\nu_{r,2}\, n(r'(s), h'(s))\, m(r'(s), h'(s)) \right\} \tag{17}$$

and

$$W = \frac{2}{R^2 H} \int_{0}^{R} r\,\mathrm{d}r \int_{0}^{H} \mathrm{d}h \left\{ \nu_{s,3}\, n^3(r,h) + 3\,\nu_{s,2}\, n(r,h)\, m(r,h) + \nu_{s,1}\, w(r,h) \right\}. \tag{18}$$

Similarly to our previous work, the above equations were solved numerically with the use of a collision number expansion method. Quantitative results will be presented below.

4 QUANTITATIVE ANALYSIS AND COMPARISON WITH THE POINT MODEL

For the quantitative calculation of the moments from Eqs. (10) - (18) and to compare them with the point model, two types of data are needed. For the former, the choice of the material composition of the item and corresponding factorial moments of the spontaneous and induced fission are needed. The same data will be used as in our previous work, assuming a sample of 20 wt% ^{240}Pu and 80 wt% ^{239}Pu, with corresponding data taken from Ref. [7]. Also, the same two cases $\alpha = 0$ and $\alpha = 0.5$ will be considered. The factorial moments of the source and induced fission neutron numbers for the two α values are shown in Table 1.

Table 1: Input parameters used in the calculations.

	First moments	Second moments	Third moments
Spontaneous fission	$\nu_{sf,1} = 2.1538$	$\nu_{sf,2} = 3.7912$	$\nu_{sf,3} = 5.2146$
Source event with $\alpha = 0.5$	$\nu_{s,1} = 1.5554$	$\nu_{s,2} = 1.8254$	$\nu_{s,3} = 2.5108$
Induced fission	$\nu_{r,1} = 3.135$	$\nu_{r,2} = 8.1162$	$\nu_{r,3} = 17.0028$

For the comparison with the point model, the first collision probability p is needed for each particular cylinder geometry. This quantity is a simplification of the point model, and it does not occur in the space-dependent calculations. However, for a fair comparison, the first collision probability used in the point model calculations must correspond to the transport model used in the space-dependent calculations. The simplest way of calculating this quantity for the cylinder

is as follows. One notes that the average escape probability $\mathrm{p_{esc}}$ of neutrons for the case of a homogeneously distributed isotropic source is equal to

$$\mathrm{p_{esc}} = \frac{1}{V}\int_V \mathrm{d}\boldsymbol{r}\, n_0(\boldsymbol{r}) \tag{19}$$

where $n_0(\boldsymbol{r})$ is shorthand for the uncollided term, Eq. (11). Hence, the first collision probability p is equal to

$$\mathrm{p} = 1-\mathrm{p_{esc}} = 1-\frac{1}{V}\int_V \mathrm{d}\boldsymbol{r}\, n_0(\boldsymbol{r}) = 1-\frac{1}{2\pi R^2\, H}\int_0^R r\,\mathrm{d}r\int_0^H \mathrm{d}h\int_{-1}^1 \mathrm{d}\mu\int_0^{2\pi}\mathrm{d}\varphi\, e^{-\ell(r,h,\mu,\varphi)} \tag{20}$$

This formula was used to calculate the first collision probability for each case.

Unlike spheres, cylinders can have various shapes corresponding to different aspect ratios H/D. In the quantitative work, 3 different shapes were used:

- a "square" cylinder, $H = D$
- a "long" cylinder, $H/D = 2.5$
- a "flat" cylinder, $H/D = 0.2$.

For each shape, the dependence of the first three factorial moments of the source event induced number distribution will be shown. However, since the same radii for the three shapes would correspond to different masses (volumes), in order for a correct comparison of the results, these will be plotted as function of a so-called "effective radius", R_{eff}. This latter is defined as the radius of an equivalent square cylinder with the same volume as the actual long and flat cylinders, respectively. In formula, one has

$$R_{eff} = R\left(\frac{H}{D}\right)^{\frac{1}{3}} \tag{21}$$

where R is the actual radius of the cylinder, and H/D is the fixed aspect ratio of the particular shape.

The dependence of the first three factorial moments on the effective radius R_{eff} (in optical units) of the cylinders with the three selected shapes is shown in Figs. 1 - 3 for both the point model and the space dependent model, for the cases $\alpha = 0$ (left figures) and $\alpha = 0.5$ (right figures). The tendencies are very similar to those observed for the sphere. For very small values of R_{eff}, the point model and space-dependent model values are both equal to the mean values of source emission particles for both values of α. As Table 1 shows, this value is smaller for the case $\alpha = 0.5$, and hence the values of the first moment remain systematically lower than those for $\alpha = 0$ for all values of R_{eff}.

With increasing radius, the values of the moments start to increase for both the point model and the space dependent model. Similarly to the case of the sphere, the moments by the space dependent model increase faster than those by the point model. The difference increases with increasing effective radius. The rate of the rise is different for the different shapes. For both the long and the flat cylinder, at the same effective radius, the moment values are lower than those of the square cylinder, the values from the long cylinder being larger than those of the flat cylinder. This because for a given effective radius the first collision probability is the largest for the square cylinder, and the smallest for the flat cylinder.

One can also note that as the order of the moments increases, both the quantitative values of the moments, as well as the difference between the point model and the space dependent

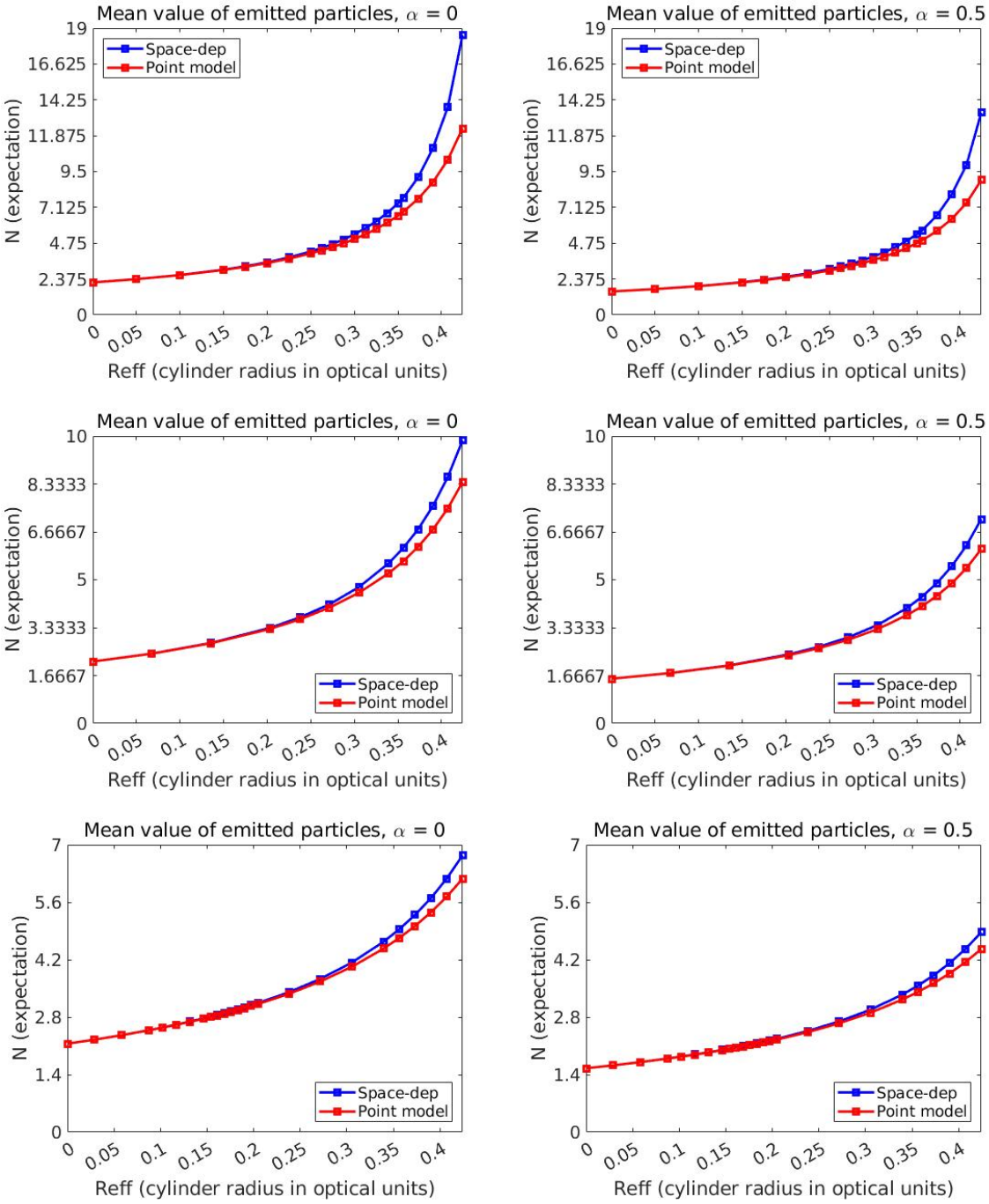

Figure 1: Mean value of emitted particles as function of cylinder effective radius for the cases $\alpha = 0$ (left) and $\alpha = 0.5$ (right). Upper figures: square cylinder; middle figures: long cylinder; bottom figures: flat cylinder.

model increases. For instance, for the third moment at $R_{eff} = 0.3$, for the square cylinder, the difference between the space dependent model and the point model exceeds 50% considerably.

The reason for the space dependent model predicting higher values for all the moments was analysed for the sphere in [3], and the same is valid for the cylinder. Namely, the space dependent model predicts a larger internal multiplication, and hence also a larger leakage multiplication than the point model.

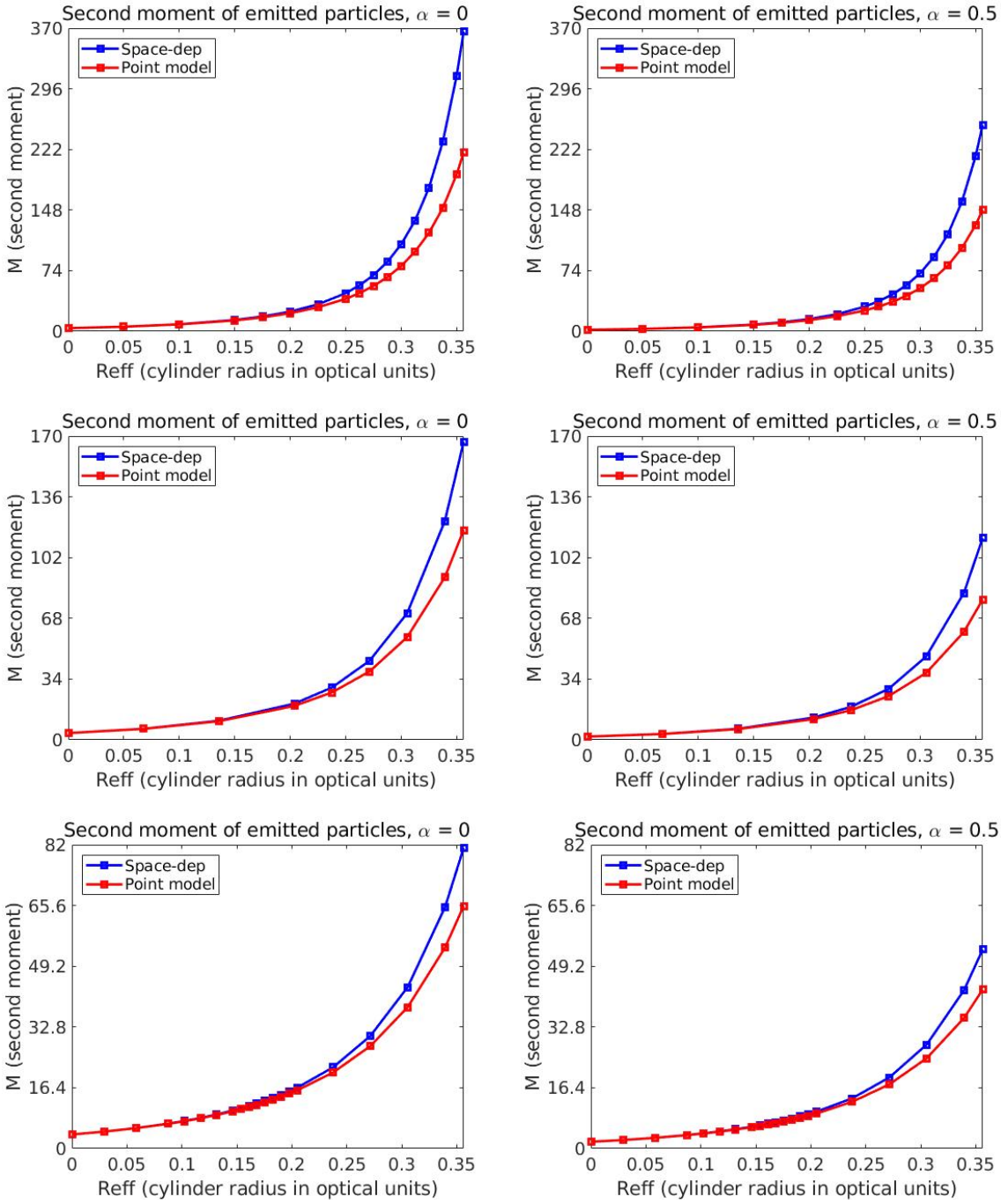

Figure 2: Second moment of emitted particles as function of cylinder effective radius for $\alpha = 0$ (left) and $\alpha = 0.5$ (right). Upper figures: square cylinder; middle figures: long cylinder; bottom figures: flat cylinder.

5 THE BIAS OF THE POINT MODEL

Since the results of both the space dependent and the point model calculation are quantitatively available, this lends a possibility to put the deviation between the two into perspective, since the space-dependent transport calculations can be expected to yield more accurate results than the point model. Hence, one can check what type of error is committed when, in evaluating a

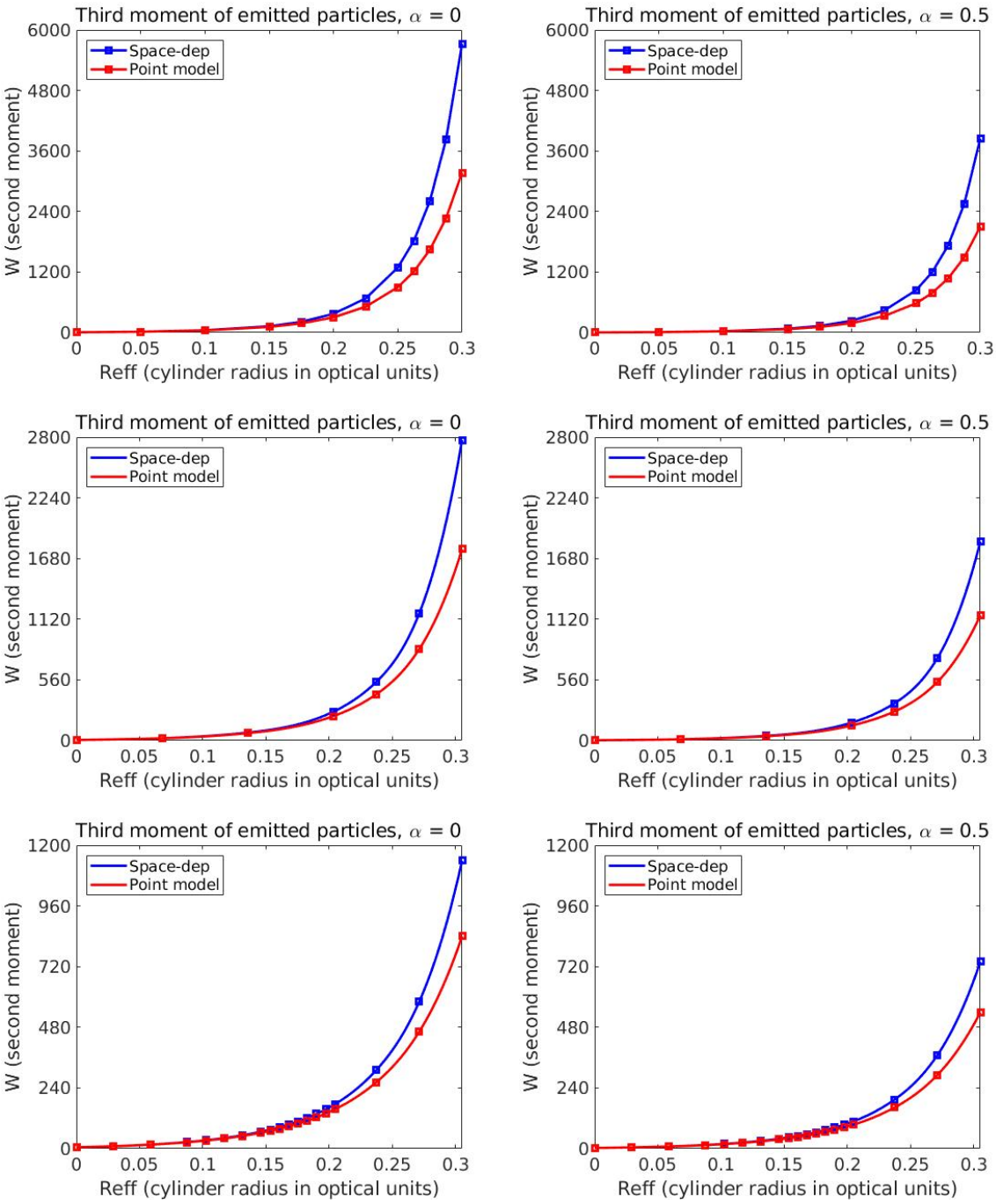

Figure 3: Third moment of emitted particles as function of cylinder effective radius for $\alpha = 0$ (left) and $\alpha = 0.5$ (right). Upper figures: square cylinder; middle figures: long cylinder; bottom figures: flat cylinder.

measurement, one uses the point model equations and the unfolding method based on them, whereas the factorial moments used in this process correspond to those given by the spade-dependent model. This is quantified by the so-called bias, which is the ratio of the results for the fission rate as derived by assuming the point model, to the correct fission rate. The procedure is quite straightforward, and is described in [3], hence it will not be described here.

For the quantification of the bias, we will compare not only the cylinders of various shapes,

but also we will make a comparison with the sphere. Such a comparison is shown in Fig. 4, displaying the bias of the point model for the case of a sphere, and the three different cylinder shapes, for both $\alpha = 0$ and $\alpha = 0.5$. The bias is shown as function of the effective radius of the items. For a correct comparison between cylinders and spheres, the effective radius for a cylinder is defined as the radius of a sphere with the same volume, i.e. the effective radius is not the same as Eq. (21), used in Figs. 1 - 3, rather in this case it is equal to

$$R_{eff} = \left(\frac{3\,H}{2\,D}\right)^{\frac{1}{3}} R. \tag{22}$$

It is seen from Fig. 4 that the bias is quite moderate for $\alpha = 0$ for all four geometries, even at quite large effective radii, but it becomes substantially larger for $\alpha = 0.5$. For $R_{eff} = 0.4$, the bias of the point model is over 30% for the sphere and for the square cylinder. It is also seen that the bias of the point model for a spherical item is very close to that of a square cylinder. This means that for the case of a square cylinder, it causes only a small error if the point model results are corrected assuming that it had a spherical shape. The results in Fig. 4 show that applying the same correction procedure would yield a much larger error (incorrect compensation of the bias of the point model) if the item was a long or a flat cylinder. On the other hand, if no correction of the bias of the point model is made, then the error in determining the fissile mass will be smaller for a flat or a long cylinder, than when the item had a spherical shape or that of a square cylinder.

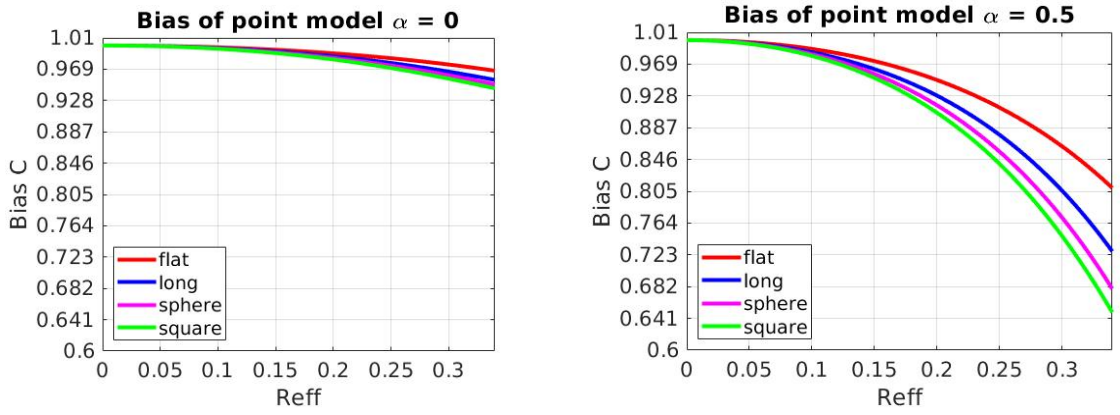

Figure 4: Bias of point model as function of the effective radius R_{eff} for $\alpha = 0$ (left figure) and $\alpha = 0.5$ (right figure), respectively.

6 CONCLUSIONS

An earlier work concerning the calculation of the multiplicity moments from a sample containing fissionable and fissile material with one-speed transport theory for a spherical item was extended to cylinders, making it possible to replace the point model equations with one-speed transport calculations for various geometries, which are supposed to give more accurate results. These more realistic results can be used to improve the results of the point model in estimating the fissile mass of a sample, e.g. by generating training sets for machine learning methods which have to replace the analytical inversion process of the point model, since the results of the space dependent model are not analytical. Work is going on in this direction and results will be reported in later publications.

ACKNOWLEDGEMENTS

The computations presented in this paper were enabled by resources provided by the Swedish National Infrastructure for Computing (SNIC) at Chalmers Centre for Computational Science and Engineering (C3SE), and at the National Supercomputer Centre (NSC), Linköping University, partially funded by the Swedish Research Council through grant agreement no. 2018-05973.

References

[1] I. Pázsit, L. Pál, and A. Enqvist, "Extension of the Böhnel model of multiplicity counting to include space- and angular de-pendence," in *Proc. INMM-60 Annual Meeting*, (paper a167, Palm Desert, CA), 14 - 18 July 2019.

[2] I. Pázsit and L. Pál, "Developments in the Calculation of the Multiplicity Moments in Space-Dependent (Non-Point) Models," in *Proc. INMM-61 Annual Meeting*, (paper a1278, Baltimore, USA), 14 - 18 July 2020.

[3] I. Pázsit and L. Pál, "Multiplicity theory beyond the point model," *Annals of Nuclear Energy*, vol. 154, p. 108119, 2021.

[4] W. Hage and D. M. Cifarelli, "On the factorial moments of the neutron multiplicity distribution of fission cascades," *Nuclear Instruments and Methods in Physics Research Section A: Accelerators, Spectrometers, Detectors and Associated Equipment*, vol. 236, no. 1, pp. 165–177, 1985.

[5] K. Böhnel, "The effect of multiplication on the quantitative determination of spontaneously fissioning isotopes by neutron correlation analysis," *Nuclear Science and Engineering*, vol. 90, pp. 75 – 82, 1985.

[6] I. Pázsit and V. Dykin, "Transport calculations of the multiplicity moments for cylinders," *Nuclear Science and Engineering*, Submitted, 2021.

[7] A. Enqvist, I. Pázsit, and S. Pozzi, "The number distribution of neutrons and gamma photons generated in a multiplying sample," *Nucl. Instr. Meth.*, vol. A 566, pp. 598 – 608, 2006.